第 34 卷第 3 期
2018 年 3 月

无 机 化 学 学 报
CHINESE JOURNAL OF INORGANIC CHEMISTRY

Vol.34 No.3
560-568

中心金属离子改变诱导 MOFs 结构和光催化性能的改变

李慧军 何亚玲 张 宁 李晴晴 徐周庆* 王 元*
(河南理工大学化学化工学院,焦作 454000)

摘要:在相同的水热条件下,铜盐、钴盐分别和配体 H_2PPCA(H_2PPCA=5-pyrazin-2-yl-1*H*-pyrazole-3-carboxylic acid)发生反应,生成了 2 个结构截然不同的金属有机配合物,分别是[Cu(PPCA)(H_2O)]·H_2O (**HPU-7**)和{[Co(PPCA)(H_2O)]·H_2O}$_n$ (**HPU-8**)。**HPU-7** 是由 $CuCl_2·2H_2O$ 与配体在 160 ℃下反应而成的,它呈现出零维的双核铜单元结构。**HPU-8** 是由 $Co(NO_3)_2·6H_2O$ 与配体在 160 ℃下反应生成的,它呈现出由双核钴单元与配体的骨架相连而成的 4,4-连接的二维层结构。中心金属离子的改变导致了不同结构 MOF 的形成,并且它们的电化学性能研究表明它们是很好的半导体材料,它们都对亚甲基蓝(MB)具有较好的光催化效果。

关键词:双核簇;2D 层;结构变化;光催化
中图分类号:O614.121;O614.81+2 **文献标识码**:A **文章编号**:1001-4861(2018)03-0560-09
DOI:10.11862/CJIC.2018.078

Structural Differences of Two MOFs Adjusted by Central Metal Ions Inducing Different Photodegradation Efficiencies

LI Hui-Jun HE Ya-Ling ZHANG Ning LI Qing-Qing XU Zhou-Qing* WANG Yuan*
(*College of Chemistry and Chemical Engineering, Henan Polytechnic University, Jiaozuo, Henan* 454000, *China*)

Abstract: By Reactions of Cu(Ⅱ), Co(Ⅱ) with H_2PPCA ligand (H_2PPCA=5-pyrazin-2-yl-1*H*-pyrazole-3-carboxylic acid) in the same hydrothermal conditions resulted in two distinct structural metal-organic frameworks (MOFs), namely, [Cu(PPCA)(H_2O)]·H_2O (**HPU-7**) and {[Co(PPCA)(H_2O)]·H_2O}$_n$ (**HPU-8**). **HPU-7** that obtained from $CuCl_2·2H_2O$ at 160 ℃ is a dinuclear cluster based on Cu(Ⅱ) ions and $PPCA^{2-}$ ligands. **HPU-8** synthesized by $Co(NO_3)_2·6H_2O$ at 160 ℃ exhibits a 4,4-connected 2D layer connected by dinuclear Co(Ⅱ) clusters and the skeletons of the $PPCA^{2-}$ ligands. The structural differences are dependent on the coordination geometries of central metal ions. And due to the structural differences, the two complexes display different photodegradation efficiencies toward methylene blue (MB). CCDC: 1575337, **HPU-7**; 1575338, **HPU-8**.

Keywords: dinuclear cluster; 2D layer; structural differences; photodegradation efficiency

0 Introduction

Recently, the rational design and construction of microporous metal-organic frameworks (MOFs) have obtained extensive attention on account of their fascinating topologies and potential applications in optical, gas storage and separation, biomimetic materials, catalysis and so on[1-4]. In particular, the assembly of MOFs showing topological complexity, aesthetic beauty, and structural integrity, especially of those with undiscovered intriguing topologies has been appealing to more and more chemists[5-8]. The controllable syntheses of MOFs are still difficult in the most of metal-organic ligands systems due to the fact that

收稿日期:2017-09-22。收修改稿日期:2017-12-14。
国家自然科学基金(No.21601050)资助。
*通信联系人。E-mail:zhqxu@hpu.edu.cn,wangyuan08@hpu.edu.cn

the assembly processes are complicated and influenced by many inner and outer factors[9-11]. Generally, the resulting framework of the MOFs depends on the structural characteristics of organic ligands, the coordination modes of metal center ions, experiment condition and the reaction pathways and so on[12-16]. In many case, metal ions can regulated the structure dramatically, which give rise to some ion-directed coordination systems. The selection of metal centers can tune the structure through their various coordination geometries[17-20].

In additional, dyes removal from contaminated water attracts the interests of the majority of researchers[21-24]. However, quickly removing the dyes from waste-water is still a challenge. Compared with absorption method, photocatalysis is one of the most effective chemical methods to alleviate the environment issue by converting inexhaustible solar energy into clean chemical substances[25-27]. Thus, the design strategy and improvement approaches for MOF-based photocatalytic activities are commendable[29-30]. It has reported that the feasible strategy of photocatalytic process is to facilitate the generation of free radical as electron acceptors to the photocatalytic reaction[31-32]. In this regard, unsaturated metal sites which could reduce charge carrier recombination probability may accelerate the generation of free radical and further degrade dye quickly. In the current study, a functional ligand with multiple coordination modes has been used as organic ligand to constructed two novel MOFs. Interestingly, their structural diversity is largely dependent on the changes of metal ions. And the two MOFs both exhibit good photocatalytic efficiency.

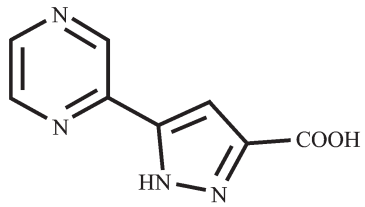

Scheme 1　Structure of the ligand

1　Experimental

1.1　Materials and measurements

All chemicals were commercially purchased. Elemental analyses for carbon, hydrogen and nitrogen were performed on a Thermo Science Flash 2000 element analyzer. FT-IR spectra were obtained in KBr disks on a PerkinElmer Spectrum One FTIR spectrophotometer in 4 000~450 cm^{-1} spectral range. The powder X-ray diffraction (PXRD) studies were performed with a Bruker AXS D8 Discover instrument (Cu $K\alpha$ radiation, λ=0.154 184 nm, U=40 kV, I=40 mA) over the 2θ range of 5°~60° at room temperature. Thermogravimetric analysis (TGA) was recorded on a Netzsch STA 449C thermal analyzer between 30 and 800 ℃ and a heating rate of 10 ℃·min^{-1} in atmosphere. Cyclic voltammetry (CV) measurements were performed on a CHI760D electrochemical workstation (Chenhua Instrument Company, ShangHai, China).

1.2　Preparations of the complexes

Synthesis of $[Cu(PPCA)(H_2O)]\cdot H_2O$ (**HPU-7**): a mixture of H_2PPCA (0.05 mmol, 10.15 mg), $CuCl_2\cdot 2H_2O$ (0.10 mmol, 17.048 mg), absolute ethanol (2 mL) and H_2O (8 mL) was placed in a Teflon-lined stainless steel vessel (25 mL), heated to 160 ℃ for 3 days, and then cooled to room temperature at a rate of 5 ℃·h^{-1}. Purple block crystals of **HPU-7** were obtained and picked out, washed with distilled water and dried in air. Elemental analysis Calcd. for $C_8H_8CuN_4O_4$(%): C 33.40, H 2.80, N 19.47. Found(%): C 33.27, H 2.87, N 20.18. IR (KBr, cm^{-1}): 3 449s, 1 611s, 1 420m, 1 279 m, 1 146m, 1 054m, 972w, 888m, 797m.

Synthesis of $\{[Co(PPCA)(H_2O)]\cdot H_2O\}_n$ (**HPU-8**): a mixture of H_2PPCA (0.05 mmol, 11.2 mg), $Co(NO_3)_2\cdot 6H_2O$ (0.10 mmol, 29.1 mg), CH_3CN (2 mL) and H_2O (8 mL) was placed in a Teflon-lined stainless steelvessel (25 mL), heated to 160 ℃ for 3 days, and then cooled to room temperature at a rate of 5 ℃·h^{-1}. Brown block crystals of **HPU-8** were obtained and picked out, washed with distilled water and dried in air. Elemental analysis Calcd. for $C_8H_8CoN_4O_4$ (%): C 33.94, H 2.85, N 19.79 . Found(%): C 33.69, H 2.47, N 20.08. IR (KBr, cm^{-1}): 3 446s, 1 611s, 1 428m, 1 370 w, 1 295m, 1 154m, 1 038m, 780m.

1.3　X-ray crystallography

X-ray Single-crystal diffraction analysis of **HPU-7** and **HPU-8** was carried out on a Bruker SMART

APEX Ⅱ CCD diffractometer equipped with a graphite monochromated Mo $K\alpha$ radiation (λ=0.071 073 nm) by using φ-ω scan technique at room temperature. The structures were solved via direct methods and successive Fourier difference synthesis (SHELXS-2014), and refined by the full-matrix least-squares method on F^2 with anisotropic thermal parameters for all non-H atoms (SHELXL-2014)[33]. The empirical absorption corrections were applied by the SADABS program[34]. The H-atoms of carbon were assigned with common isotropic displacement factors and included in the final refinement by the use of geometrical restraints. H-atoms of water molecules were first located by the Fourier maps, then refined by the riding mode. The crystallographic data for **HPU-7** and **HPU-8** are listed in Table 1. Moreover, the selected bond lengths and bond angles are listed in Table 2.

CCDC: 1575337, **HPU-7**; 1575338, **HPU-8**.

Table 1 Crystal data and structure refinement parameters for HPU-7 and HPU-8

Complex	HPU-7	HPU-8
Empirical formula	$C_8H_8CuN_4O_4$	$C_8H_8CoN_4O_4$
Formula weight	287.73	283.11
Temperature / K	296	296
Crystal system	Monoclinic	Monoclinic
Space group	$P2_1/c$	$P2_1/c$
a / nm	0.788 91(13)	0.854 8(4)
b / nm	0.719 49(12)	1.372 0(6)
c / nm	1.831 4(3)	0.930 5(4)
β / (°)	100.825(3)	115.634(5)
Volume / nm^3	1.021 0(3)	0.983 9(8)
Z	4	4
D_c / (g·cm^{-3})	1.872	1.911
μ / mm^{-1}	2.149	1.755
Crystal size / mm	0.30×0.20×0.20	0.30×0.20×0.20
R_{int}	0.033 0	0.022 1
F(000)	580.0	572.0
Reflection collected, unique	5 049, 1 804	4 906, 1 731
Goodness-of-fit on F^2	1.033	1.049
Final R indices [$I>2\sigma(I)$]	R_1=0.029 5, wR_2=0.066 5	R_1=0.024 1, wR_2=0.057 7
R indices (all data)	R_1=0.040 2, wR_2=0.071 7	R_1=0.028 0, wR_2=0.060 1

Table 2 Selected bond lengths (nm) and angles (°) for HPU-7 and HPU-8

HPU-7					
Cu(1)-N(1)^i	0.192 6(2)	Cu(1)-N(2)	0.192 9(2)	Cu(1)-O(1)^i	0.199 4(2)
Cu(1)-N(3)	0.206 2(2)	Cu(1)-O(3)	0.239 8(2)	N(1)-Cu(1)^i	0.192 6(2)
O(1)-Cu(1)^i	0.199 4(2)				
C(1)-O(1)-Cu(1)^i	116.00(17)	N(1)^i-Cu(1)-N(2)	94.14(9)	N(1)^i-Cu(1)-O(1)^i	80.56(9)
N(2)-Cu(1)-O(1)^i	173.35(9)	N(1)^i-Cu(1)-N(3)	172.41(10)	N(2)-Cu(1)-N(3)	79.23(10)
O(1)^i-Cu(1)-N(3)	105.77(9)	N(1)^i-Cu(1)-O(3)	100.34(9)	N(2)-Cu(1)-O(3)	94.33(9)
O(1)^i-Cu(1)-O(3)	90.59(8)	N(3)-Cu(1)-O(3)	83.98(9)	Cu(1)-O(3)-H(3A)	109.7
Cu(1)-O(3)-H(3B)	108.1				
HPU-8					
Co(1)-N(4)^i	0.202 9(5)	Co(1)-N(3)	0.203 3(5)	Co(1)-O(1)^i	0.213 3(5)

Continued Table 2

Co(1)-O(3)	0.215 8(5)	Co(1)-N(2)^{ii}	0.218 7(6)	Co(1)-N(1)	0.220 6(5)
N(2)-Co(1)^{iii}	0.218 7(5)	N(4)-Co(1)^{i}	0.202 9(5)	O(1)-Co(1)^{i}	0.213 3(5)
N(4)^{i}-Co(1)-N(3)	94.8(2)	N(4)^{i}-Co(1)-O(1)^{i}	76.87(19)	N(3)-Co(1)-O(1)^{i}	171.61(19)
N(4)^{i}-Co(1)-O(3)	94.1(2)	N(3)-Co(1)-O(3)	92.5(2)	O(1)^{i}-Co(1)-O(3)	88.99(18)
N(4)^{i}-Co(1)-N(2)^{ii}	95.4(2)	N(3)-Co(1)-N(2)^{ii}	92.6(2)	O(1)^{i}-Co(1)-N(2)^{ii}	87.37(19)
O(3)-Co(1)-N(2)^{ii}	168.76(19)	N(4)^{i}-Co(1)-N(1)	170.3(2)	N(3)-Co(1)-N(1)	75.7(2)
O(1)^{i}-Co(1)-N(1)	112.63(19)	O(3)-Co(1)-N(1)	88.08(19)	N(2)^{ii}-Co(1)-N(1)	83.5(2)
C(1)-N(1)-Co(1)	129.3(4)	C(4)-N(1)-Co(1)	113.5(4)	C(2)-N(2)-Co(1)^{iii}	122.3(4)
C(3)-N(2)-Co(1)^{iii}	120.5(4)	C(5)-N(3)-Co(1)	120.4(4)	N(4)-N(3)-Co(1)	131.5(4)
C(7)-N(4)-Co(1)^{i}	117.5(4)	N(3)-N(4)-Co(1)^{i}	133.6(4)	C(8)-O(1)-Co(1)^{i}	116.4(4)
Co(1)-O(3)-H(3A)	113.0	Co(1)-O(3)-H(3B)	113.9		

Symmetry codes: ^{i} $-x+1, -y, -z+2$ for **HPU-7**; ^{i} $-x+1, -y, -z+1$; ^{ii} $x, -y+0.5, z+0.5$; ^{iii} $x, -y+0.5, z-0.5$ for **HPU-8**.

1.4 Photocatalytic degradation of methylene blue (MB)

The procedure was as follows: 30 mg of the dissolved **HPU-7** or **HPU-8** was dispersed into 100 mL of MB aqueous solution (12.75 mg·L^{-1}), followed by the addition of four drops of hydrogen peroxide solution (H_2O_2, 30%). The suspensions were magnetically stirred in the dark for over 1 h to ensure adsorption equilibrium of MB onto the surface of samples. And a 2.6 nm xenon arc lamp was used as a light source. An optical filter in the equipment of xenon arc lamp was used to filtering out the UV emission below 400 nm. Visible light then irradiated the above solutions for every 10 min until 110 min, and the corresponding reaction solutions were filtered and the absorbance of MB aqueous solutions was then measured by a spectrophotometer. For comparison, the contrast experiment was completed under the same conditions without any catalysts. The characteristic peak (λ=660 nm) for MB was employed to monitor the photocatalytic degradation process.

2 Results and discussion

2.1 Crystal structures of complexes HPU-7 and HPU-8

Single-crystal X-ray measurement reveals that **HPU-7** crystallizes in the monoclinic space group $P2_1/c$. Its asymmetric unit consists of one Cu(Ⅱ), one $PPCA^{2-}$ ligands and two water molecules. As shown in Fig.1a, the Cu1 ion is five-coordinated by three N atoms from two ligands, two oxygen atoms from the carboxylic group of the ligand and water molecule creating the distorted tetragonal pyramid geometry. The carboxylate group of the $PPCA^{2-}$ ligand adopts μ_1-:η^1:η^1 coordination mode. The ligand ligates with two Cu(Ⅱ) ions using its two nitrogen atoms (N1 and N2) and one oxygen atom (O1) forming a two nuclear $[Cu_2(PPCA)_2(H_2O)_2]$ unit. In the binuclear unit, the distance of adjacent Cu atoms is 0.395 31 nm. And then the adjacent nuclear units are linked through hydrogen bonds (O3–H3…N4 and O1W–H1B…O1) (Fig.1b) resulting in a two-dimensional supramolecular architecture in Fig.1c.

Single-crystal X-ray measurement reveals that **HPU-8** crystallizes in the monoclinic space group $P2_1/c$. Its asymmetry unit includes one Co(Ⅱ), one H_2PPCA ligand and two water molecules. As shown in Fig.2a, Co(Ⅱ) ion in a distorted octahedral environment is completed by four nitrogen atoms from three ligands, two oxygen atoms from a water molecule and the carboxylic group of one ligand. The ligand coordinates to three Co(Ⅱ) ions with its four nitrogen atoms and one oxygen atom (O1). Adjacent Co(Ⅱ) ions are connected by -N-N- bridges giving rise to binuclear units with the distances between Co…Co of 0.409 21 nm. It is different from the structure of **HPU-7** that the N atom of pyrazine also participates in the coordination. Therefore, the binuclear units are connected

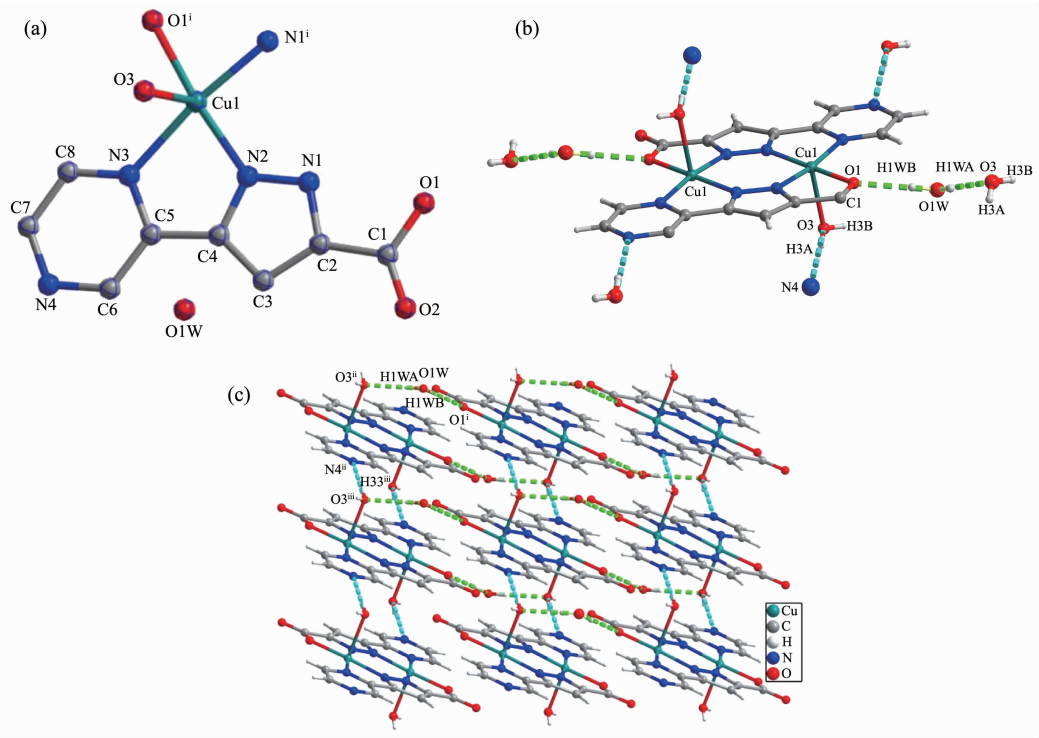

Symmetry code: [i] $-x, -1+y, -1+z$; [ii] $1+x, -1+y, -1+z$; [iii] $1-x, -1+y, 1-z$; [iv] $0.5-x, -2.5+y, 0.5-z$; [v] $x, -2+y, -1+z$

Fig.1 (a) Coordination environment of Cu(Ⅱ) ion in **HPU-7** with hydrogen atoms omitted for clarity; (b) Hydrogen bonds in **HPU-7**; (c) 2D supramolecular architecture connected by hydrogen bonds in **HPU-7**

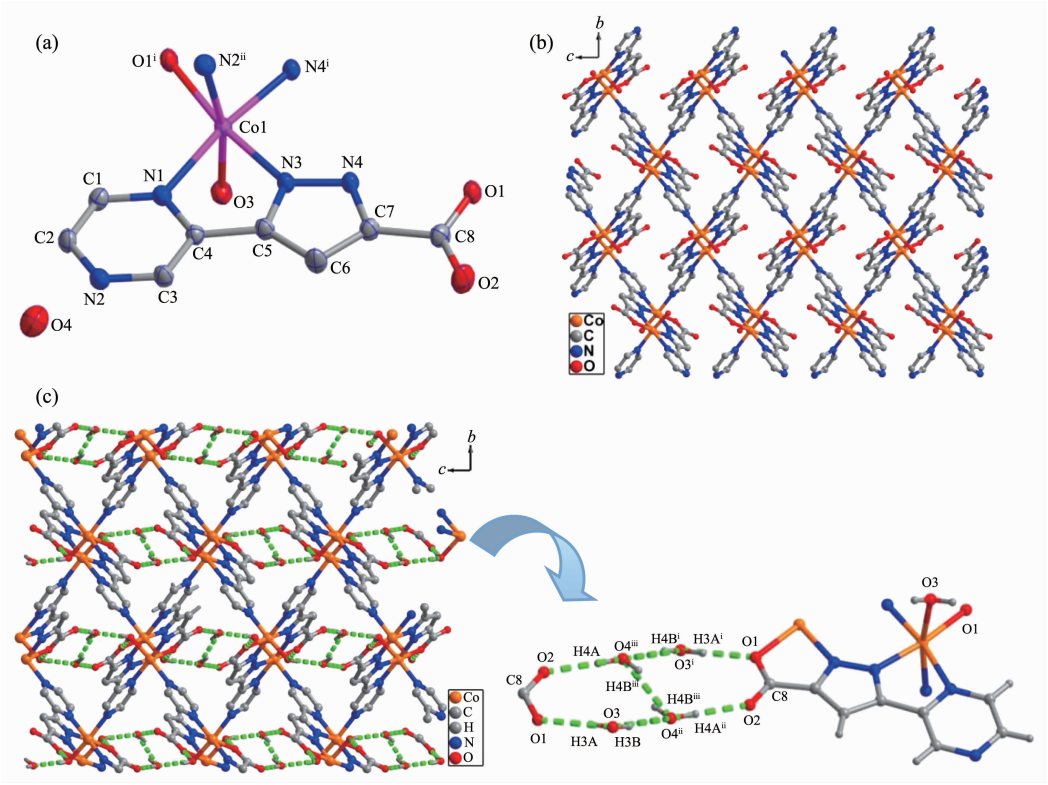

Symmetry code: [i] $-1+x, y, z$; [ii] $-x, 1-y, -z$; [iii] $-1+x, -1+y, z$

Fig.2 (a) Coordination environment of Co(Ⅱ) ion in **HPU-8**; (b) 2D layer of **HPU-8**; (c) 3D architecture connected by hydrogen bonds

together forming a two-dimensional network structure, as shown in Fig.2b. Besides, there is guest water molecules embedded in adjacent layers, which generates hydrogen bonds with other O atoms. Furthermore, the adjacent layers are connected together by these hydrogen bonds resulting in a three-dimensional supramolecular architecture in Fig.2d.

2.2 PXRD patterns and thermal stability analysis

To confirm the phase purity of the two complexes, the PXRD patterns were recorded for **HPU-7** and **HPU-8**, and they were comparable to the corresponding simulated ones calculated from the single crystal diffraction data (Fig.3), indicating a pure phase of each bulky sample.

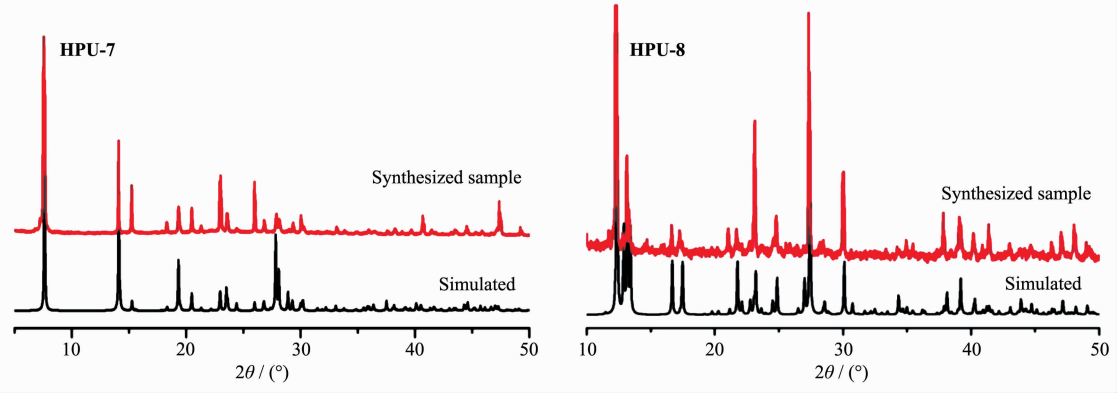

Fig.3　Powder XRD patterns for **HPU-7** and **HPU-8**

As shown in Fig.4, **HPU-7** show the first weight loss of 12.67% corresponding to the release of both guest and coordinated two water molecules (Calcd. 12.51%). Then, the framework is stable up to about 414 ℃. For **HPU-8**, the gradual weight change before 90 ℃ is attributed to the removal of both guest and coordinated two water molecules (12.89%, Calcd. 12.71%). Then, the major weight loss occurs in next step above 407 ℃, which may be ascribed to the decomposition of the coordination framework.

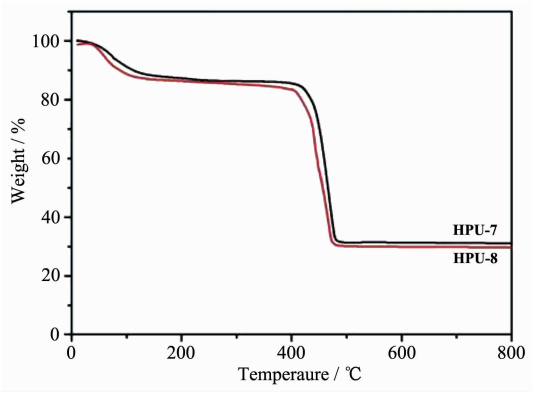

Fig.4　TG curves of the complexes **HPU-7** and **HPU-8**

2.3 Physical characterizations

To study the electrochemical synthesis of **HPU-7** and **HPU-8**, cyclic voltammetry is performed using standard electrochemical equipment within the scan rate of 20 mV·s^{-1} and potential range of −1 to 0.36 V. The CV curves show that **HPU-7** and **HPU-8** have good conductivities (Fig.5). Besides, Mott-Schottky

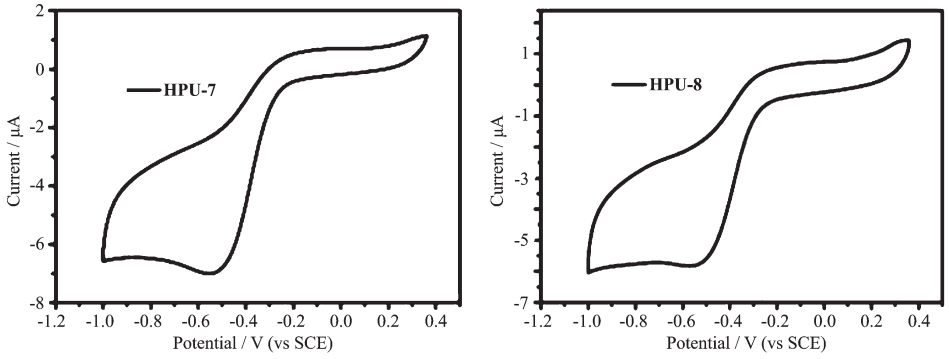

Scan rate: 20 mV·s^{-1}

Fig.5　CV curves of **HPU-7** and **HPU-8** in 0.1 mol·L^{-1} KOH solution

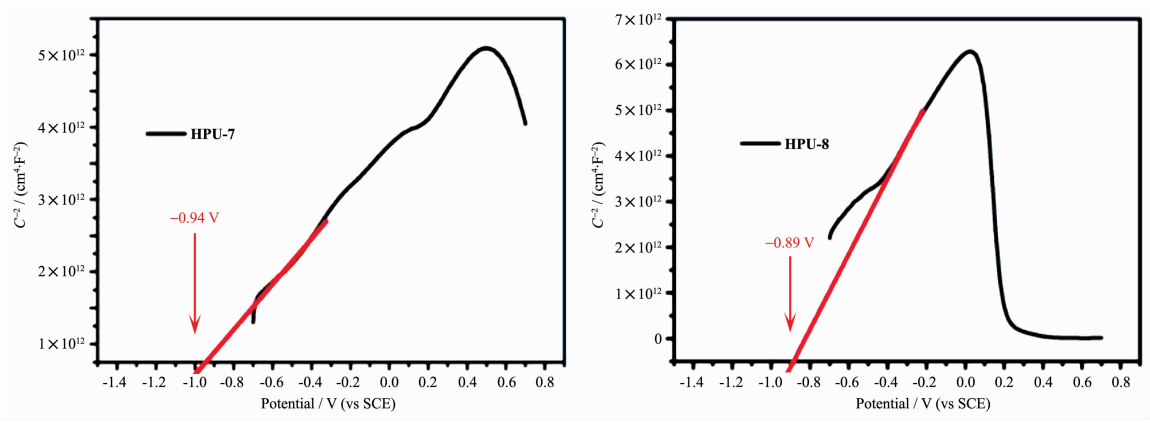

Fig.6 Mott-Schottky plots of **HPU-7** and **HPU-8** in 0.1 mol·L^{-1} KOH aqueous solution

measurements were also conducted for better understanding the intrinsic electronic properties of the two complexes. As shown in Fig.6, the slope of C^{-2} values versus potential are observed indicating that both the two complexes show n-type semiconductors. The flat-bands potential of **HPU-7** and **HPU-8** determined from Mott-Schottky plots are −0.94 and −0.89 V, respectively, versus Hg/Hg_2Cl_2 electrode at pH 13.0. So the redox potential of the conduction bands of **HPU-7** and **HPU-8** are −0.70 and −0.65 V versus normal hydrogen electrode (NHE).

2.4 Photocatalytic experiments

Photocatalysts have attracted much attention due to their potential applications in purifying water and air by thoroughly decomposing organic compounds. To evaluate the photocatalytic performance of these

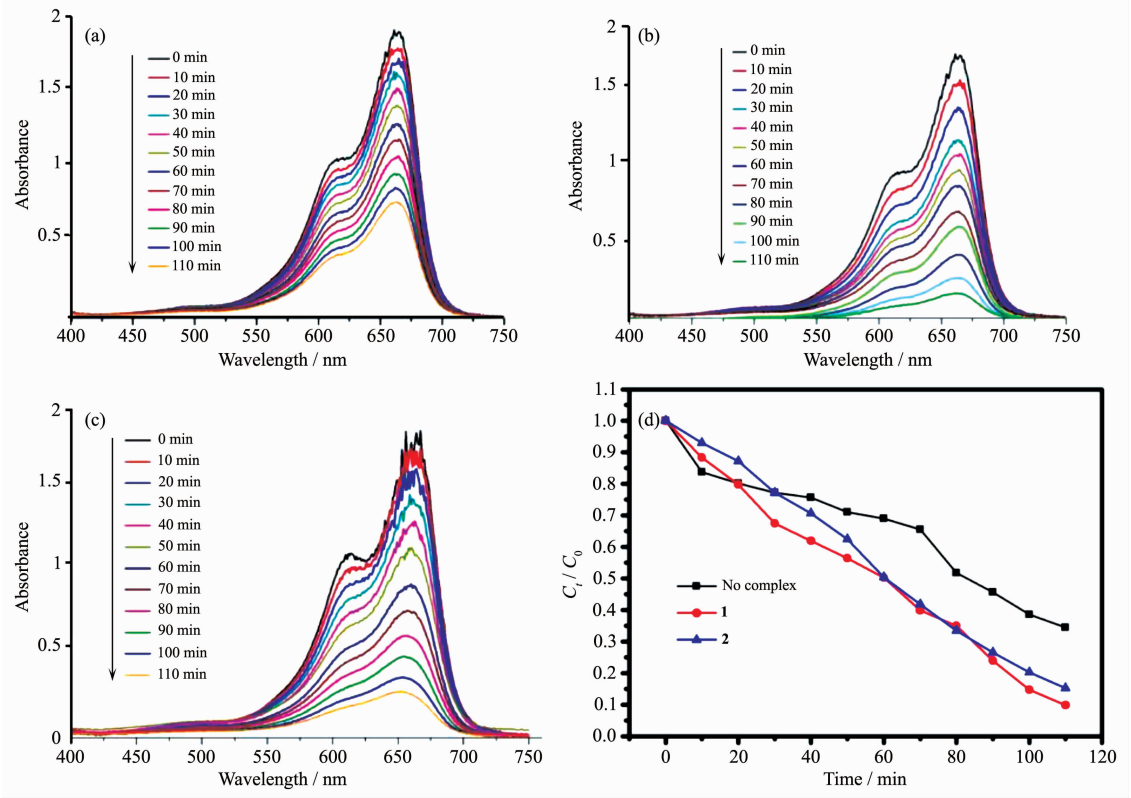

Fig.7 UV-Vis absorption of MB at different time intervals under high-pressure Hg lamp irradiation without (a) or with complexes **HPU-7** (b) and **HPU-8**(c) as catalysts, respectively; (d) Plots of C_t/C_0 vs time for MB degradation without or with complexes **HPU-7** and **HPU-8**

complexes, the photocatalytic degradation of MB aqueous solution was performed at ambient temperature. And the concentrations of MB versus reaction time of no complex and **HPU-7** and **HPU-8** are drawn in Fig.7.

As shown in the Fig.7, with the gradient changes of reaction time, both of the absorbency of the solution is gradually reduced at 660 nm. The degradation rate is defined as $(1-C_t/C_0)\times100\%$, where C_t and C_0 represent the remnant and initial concentration of MB respectively. Without addition of these complexes, the MB degradation rate was only 59.14%. After addition of **HPU-7** and **HPU-8**, the MB degradation rates were 90.61% and 85.34% for **HPU-7** and **HPU-8**, respectively. Therefore it was found that **HPU-7** has better photocatalytic degradation efficiency.

These results suggest that **HPU-7** may be better candidate for photocatalytic degradation of MB. As mentioned in literature[35-36], the photocatalytic mechanism is clarified as below: the electrons of the complex could be excited from the valence band (VB) to the conduction band (CB). Then, the equal amount of positive vacancies is left in VB (h^+). Besides, O_2 or hydroxyl (OH^-) absorbed on the surfaces of the photocatalysts could interact with the electrons (e^-) on the CB or the hole (h^+) on the VB, respectively, which give rise to hydroxyl radicals (OH). As is known, the OH radical is the important factor for cleaving MB effectively in the above photocatalytic process. So the release difficulty of OH radicals determines the catalytic effects. OH radicals are generated by oxygenating H_2O_2, which are deactivated by photocatalyst generating LMCT. Therefore, the structures of photocatalyst are the crucial issues for the faster generation speed of OH radicals. By comparison, **HPU-7** owns more unsaturated metal sites which could reduce charge carrier recombination probability and generate OH radicals more easily. So **HPU-7** shows better photocatalytic degradation efficiency.

3 Conclusions

In summary, two new MOFs based on a multifunctional ligand were successfully synthesized, which display diverse structures from 0D to 2D frameworks. The pyrazinyl functional groups could adjust coordination numbers ligating to different metal ions, which contribute to the formation of different structural MOFs. In addition, their electrochemical properties are also studied. The result shows that they have good conductivities. So they both show good photocatalytic efficiencies for the decomposition of MB. Besides, **HPU-7** with unsaturated metal sites could reduce charge carrier recombination probability and exhibit better photocatalytic efficiency. Further research is underway to synthesize other materials with better application in decomposing other dyestuff.

References:

[1] Yang H, Wei Y L, Dong X Y, et al. *Chem. Mater.*, **2015**,**27**: 1327-1331

[2] Wei Y S, Hu X P, Han Z, et al. *J. Am. Chem. Soc.*, **2017**, **139**:3505-3512

[3] WANG Qiang(王强), XU Rui(徐睿), WANG Xu-Sheng(王旭生), et al. *Chinese J. Inorg. Chem.*(无机化学学报), **2017**,**33** (11):2038-2044

[4] JI Qing-Yan(季卿妍), WANG Qian(王倩), LI Hong-Xin(李洪昕), et al. *Chinese J. Inorg. Chem.*(无机化学学报), **2017**, **33**(11):2031-2037

[5] Gao M L, Cao X M, Zhang Y Y, et al. *RSC Adv.*, **2017**,**7**: 45029-45033

[6] Li Z X, Liu X F, Ling Y, et al. *Inorg. Chem. Commun.*, **2017**,**84**:59-62

[7] Murinzi T W, Hosten E, Watkins G M. *Polyhedron*, **2017**, **137**:188-196

[8] Li S B, Zhang L, Wang J X, et al. *Inorg. Chem. Commun.*, **2017**,**82**:57-60

[9] Li H J, Wang Y, Cai H X, et al. *RSC Adv.*, **2015**,**5**:89833-89838

[10]Meng W, Xu S, Dai L, et al. *Electrochim. Acta*, **2017**,**230**: 324-332

[11]Guo X H, Li Y S, Peng Q Y, et al. *Polyhedron*, **2017**,**133**: 238-244

[12]Li T T, Liu Y M, Wang T, et al. *Inorg. Chem. Commun.*, **2017**,**84**:5-9

[13]Cai S L, Huang Y, Gao Y, et al. *Inorg. Chem. Commun.*, **2017**,**84**:10-14

[14]Wu Z F, Guo L K, Huang X Y, et al. *Inorg. Chem.*, **2017**, **56**:7397-7403

[15]Park J, Oh M. *Nanoscale*, **2017**,**9**:12850-12854

[16]Rajak R, Saraf M, Mohammad A, et al. *J. Mater. Chem. A*, **2017**,**5**:17998-18011

[17]Hou J Y, Luan Y, Huang X B, et al. *New J. Chem.*, **2017**, **41**:9123-9129

[18]Zhao H M, Xia Q S, Xing H Z, et al. *ACS Sustainable Chem. Eng.*, **2017**,**5**:4449-4456

[19]Tan Y X, Zhang Y, He Y P, et al. *Inorg. Chem.*, **2014**,**53**: 12973-12976

[20]Dey A, Konavarapu S K, Sasmal H S, et al. *Cryst. Growth Des.*, **2016**,**16**:5976-5984

[21]Meng X M, Zhang X Y, Wang X P, et al. *Polyhedron*, **2017**, **137**:81-88

[22]Liu C B, Sun H Y, Li X Y, et al. *Inorg. Chem. Commun.*, **2014**,**47**:80-83

[23]Liu D M, Xie Z G, Ma L Q, et al. *Inorg. Chem.*, **2010**,**49**: 9107-9109

[24]Ahmed A, Forster M, Jin J S, et al. *ACS Appl. Mater. Interfaces*, **2015**,**7**:18054-18063

[25]Peng Y G, Huang H L, Liu D H, et al. *ACS Appl. Mater. Interfaces*, **2016**,**8**:8527-8535

[26]Fan L Y, Yu K, Lv J H, et al. *Dalton Trans.*, **2017**,**46**:10355 -10363

[27]Bibi R, Wei L F, Shen Q H, et al. *J. Chem. Eng. Data*, **2017**,**62**:1615-1622

[28]Li Q, Xue D X, Zhang Y F, et al. *J. Mater. Chem. A*, **2017**, **5**:14182-14189

[29]Xia Q S, Yu X D, Zhao H M, et al. *Cryst. Growth Des.*, **2017**,**17**:4189-4195

[30]He Y, Xu T, Hu J, et al. *RSC Adv.*, **2017**,**7**:30500-30505

[31]Wang X L, Sun J J, Lin H Y, et al. *CrystEngComm*, **2017**, **19**:3167-3177

[32]Li L J, Yang L K, Chen Z K, et al. *Inorg. Chem. Commun.*, **2014**,**50**:62-64

[33]Sheldrick G M. *Acta Crystallogr. Sect. C*: *Cryst. Struct. Commun.*, **2015**,**C71**:3-8

[34]Sheldrick G M. *SADABS*, University of Göttingen, Germany, **1996**.

[35]Li H J, He Y L, Zhao W L, et al. *Polyhedron*, **2017**,**133**: 412-418

[36]Wang X L, Luan J, Sui F F, et al. *Cryst. Growth Des.*, **2013**, **13**:3561-3576